photonics

MDPI

Review

Temporal Reflection from Ultrashort Solitons in Nonlinear Dispersive Medium: Impact of Raman Scattering

Govind P. Agrawal

The Institute of Optics, University of Rochester, Rochester, NY 14627, USA; govind.agrawal@rochester.edu

Abstract: This review focuses on phenomena such as temporal reflection, total internal reflection, and waveguiding from ultrashort solitons forming inside a nonlinear dispersive medium such as an optical fiber. The case of wider solitons, moving at a constant speed inside the fiber, is discussed first to introduce the basic concepts. In the case of short solitons, the phenomenon of intrapulse Raman scattering shifts their spectrum toward longer wavelengths and decelerates them as they propagate through an optical fiber. These features lead to several novel effects such as temporal focusing and waveguiding by a single variable-speed Raman soliton. Recent experimental results are also discussed in this context.

Keywords: optical fibers; Raman scattering; solitons; temporal reflection

1. Introduction

Considerable attention has been paid recently to optical waves propagating in a medium whose refractive index (or electric permittivity) varies with time [1–6], although such a medium was studied as early as 1958 [7]. In most cases, the refractive index of the time-varying medium is assumed to be modulated temporally in a spatially uniform fashion on the time scale of a single cycle of the optical field incident on it. By changing the medium's refractive index in a periodic fashion, it is even possible to form a photonic time crystal [8–10]. As it is difficult to produce rapid index changes all across a medium on femtosecond time scales, experiments have involved low frequencies using water waves [11], microwaves [12], or ultra-cold atoms [13]. Further, the effects of chromatic dispersion, neglected in most theoretical studies, should be considered for any dielectric medium with a time-varying refractive index.

The technique of traveling-wave modulation provides a solution to such issues. In this case, changes in the refractive index of a dispersive medium move at the speed of the traveling wave used to create them [14–16]. Since the refractive index of the medium varies both in space and time, we refer to it as a spatiotemporal dispersive medium. The simplest situation, shown schematically in Figure 1, corresponds to a moving boundary (thick black line) with different refractive indices on its two sides. When an optical pulse interacts with this boundary inside a dispersive medium, it splits into two pulses, whose spectra are shifted such that they travel at different speeds [16–19]. These pulses represent the transmitted and reflected pulses and are temporal analogs of the reflection and refraction at a spatial interface [14]. This type of temporal reflection does not require index modulation to occur on a single-cycle time scale. Further, it is possible to obtain a temporal analog of total internal reflection and to use it for time-domain waveguiding [16].

A moving index boundary can be obtained using the optical Kerr effect. In this case, intense pump pulses are launched into a nonlinear dispersive medium, such as an optical fiber, to propagate as optical solitons [20]. The fiber's refractive index increases in a time window set by the width of the solitons, and this window moves at the speed of pump pulses. When a probe pulse, moving at a different speed because of its different wavelength, interacts with this high-index window, a reflected pulse is generated at a wavelength shifted

Citation: Agrawal, G.P. Temporal Reflection from Ultrashort Solitons in Nonlinear Dispersive Medium: Impact of Raman Scattering. *Photonics* **2024**, *11*, 1189. https://doi.org/10.3390/photonics11121189

Received: 25 November 2024
Revised: 12 December 2024
Accepted: 13 December 2024
Published: 19 December 2024

from that of the probe [17]. A pump–probe configuration has been used for *nonlinear fiber optics* in many different contexts and was used to obtain an optical analog of the event horizon associated with a black hole [21–24].

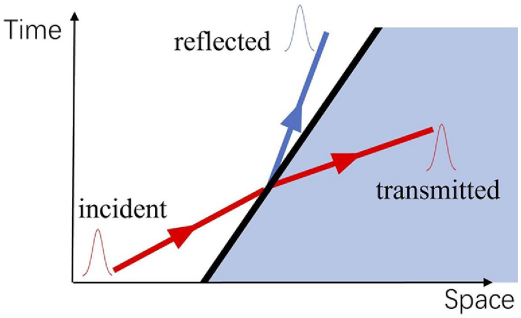

Figure 1. Temporal analogs of reflection and refraction at a moving temporal boundary (thick black line) with different refractive indices on its two sides. Arrows indicate the incident, reflected, and transmitted pulses.

When the width of pump pulses exceeds a few picoseconds, the shape and width of solitons do not change with propagation along an optical fiber. However, shorter pump pulses (width of 100 fs or less) are often employed in practice because their use reduces the length of fiber needed for experiments. In this situation, higher-order effects begin to affect the solitons. The most relevant higher-order nonlinear effect turned out to be a phenomenon known as intrapulse Raman scattering [20]. This effect shifts the soliton's spectrum toward longer wavelengths in a continuous fashion, which, in turn, causes the soliton to decelerate as it propagates down the fiber. The net effect is that the speed of the moving temporal boundary keeps decreasing inside the fiber. This review focuses on the impact of such a boundary on temporal reflection and time-domain waveguiding.

This review is organized as follows. Section 2 focuses first on the case of relatively wide solitons, moving at a constant speed inside the fiber, and introduces the basic concepts behind time-domain reflection and waveguiding. Section 3 shows how these phenomena are modified for shorter solitons by including the impact of intrapulse Raman scattering. Temporal waveguiding of a probe pulse by two short solitons is also considered in this section. The focus of Section 4 is on a new kind of waveguiding, where multiple temporal reflections from a single decelerating soliton guide the probe pulse along its trajectory. Numerical simulations and experiments reveal that different spectral shifts induced during such reflections can be used to deduce the internal trajectory of the soliton from the data taken at the output end of a fiber. The main conclusions are summarized in Section 5.

2. Solitons Acting as Mirrors

In general, pump pulses launched into an optical fiber become distorted because of the dispersive and nonlinear effects, resulting in a high-index region that does not maintain itself over the fiber's length. This problem can be solved by making use of optical solitons, forming when pump pulses are launched at a wavelength longer than the zero-dispersion wavelength of the fiber so that the group-velocity dispersion (GVD) is anomalous at the pump's wavelength.

2.1. Temporal Reflection

In this section, we consider the case of picosecond pump pulses, which can form ideal solitons that travel at a constant speed inside an optical fiber. Such pulses evolve according to the well-known nonlinear Schrödinger (NLS) equation [20],

$$\frac{\partial A_p}{\partial z} + \frac{i\beta_{2p}}{2}\frac{\partial^2 A_p}{\partial T^2} = i\gamma_p |A_p|^2 A_p, \tag{1}$$

where A_p is the slowly varying amplitude, $T = t - z/v_p$ is time measured in a frame moving at the speed v_p of pump pulses, and β_{2p} is the GVD parameter at the pump's wavelength. The formation of solitons requires β_{2p} to be negative. It also requires that the width and peak power (T_s and P_s) of pump pulses are chosen such that $N^2 = \gamma P_s T_s^2/|\beta_{2p}| = 1$, where N is the soliton's order. The nonlinear parameter γ_p is related to the Kerr coefficient n_2 as $\gamma = \omega_p n_2/(cA_{\text{eff}})$, where A_{eff} is the effective area of the single mode supported by the fiber. The fiber's losses are neglected in Equation (1), as lengths shorter than 1 km are employed in practice.

When Equation (1) is solved with the initial condition, $A_p(0) = \sqrt{P_s}\,\text{sech}(T/T_s)$, and P_s is chosen such that $N = 1$, each pump pulse forms a fundamental soliton, whose shape, width, and peak power do not change with z. In this situation, the fiber's refractive index n increases by a small amount (typically $< 10^{-6}$) over the soliton's duration and is the largest at the peak of the soliton. This increase in n creates a spatiotemporal boundary, moving at the speed of pump pulses. A probe pulse sees this increase through $\beta_b = 2\gamma|A_p|^2$ [20], where the factor of two results from the nonlinear phenomenon of cross-phase modulation (XPM).

The probe's evolution is governed by an equation similar to Equation (1), after the nonlinear term on its right side is replaced with the XPM term as follows:

$$\frac{\partial A}{\partial z} + \Delta\beta_1 \frac{\partial A}{\partial T} + \frac{i\beta_2}{2}\frac{\partial^2 A}{\partial T^2} = 2i\gamma|A_p|^2 A, \tag{2}$$

where $\Delta\beta_1 = \beta_1 - 1/v_p$ accounts for the speed difference between the pump and probe pulses. The parameters β_2 and γ are taken at the probe's wavelength. It is useful to introduce two normalized variables, such as $\tau = T/T_0$ and $\xi = z/L_D$, where $L_D = T_0^2/|\beta_2|$ is the dispersion length. The resulting equation for the probe pulse is

$$\frac{\partial A}{\partial \xi} + d\frac{\partial A}{\partial \tau} + \frac{i}{2}\frac{\partial^2 A}{\partial \tau^2} = iC_x \text{sech}^2(\tau/\tau_s)A, \tag{3}$$

where $d = \Delta\beta_1 L_D$, $\tau_s = T_s/T_0$, and $C_x = 2\gamma P_s L_D$ are three dimensionless parameters. This equation is solved numerically to study the evolution of a probe pulse and its interaction with a pump soliton inside a silica fiber. In the moving fame, the soliton's peak remains fixed at $\tau = 0$.

Figure 2 shows the temporal reflection and refraction of a Gaussian probe pulse using $d = 30$ and $C_x = 500$, occurring when it collides with a soliton whose width is 10 times shorter than its own width ($\tau_s = 0.1$). For comparison, the bottom part shows what happens when the soliton is wider by a factor of two ($\tau_s = 0.2$). When a soliton is used to form a spatiotemporal boundary, its width plays an important role because it dictates the sharpness of this boundary. A shorter soliton produces a sharer boundary. One may naively think that reflection would be reduced for a wider soliton. However, as seen in Figure 2, the opposite happens: reflectivity increases from 75% to nearly 95% when the width of the soliton doubles. When the soliton-induced index change is large enough, the temporal analog of total internal reflection (TIR) occurs, which can be exploited for making time-domain waveguides. A temporal analog of Goos–Hänchen shift also occurs during this phenomenon.

The impact of a boundary's sharpness on temporal reflection was studied in 2021 using a transfer-matrix approach with a staircase model [19]. The results show that the frequency range over which reflection can occur is reduced as the rise time increases. However, TIR persists even for shallow boundaries with long rise times. This feature suggests that solitons can be used as time-domain mirrors even when pump pulses have relatively long rise and fall times.

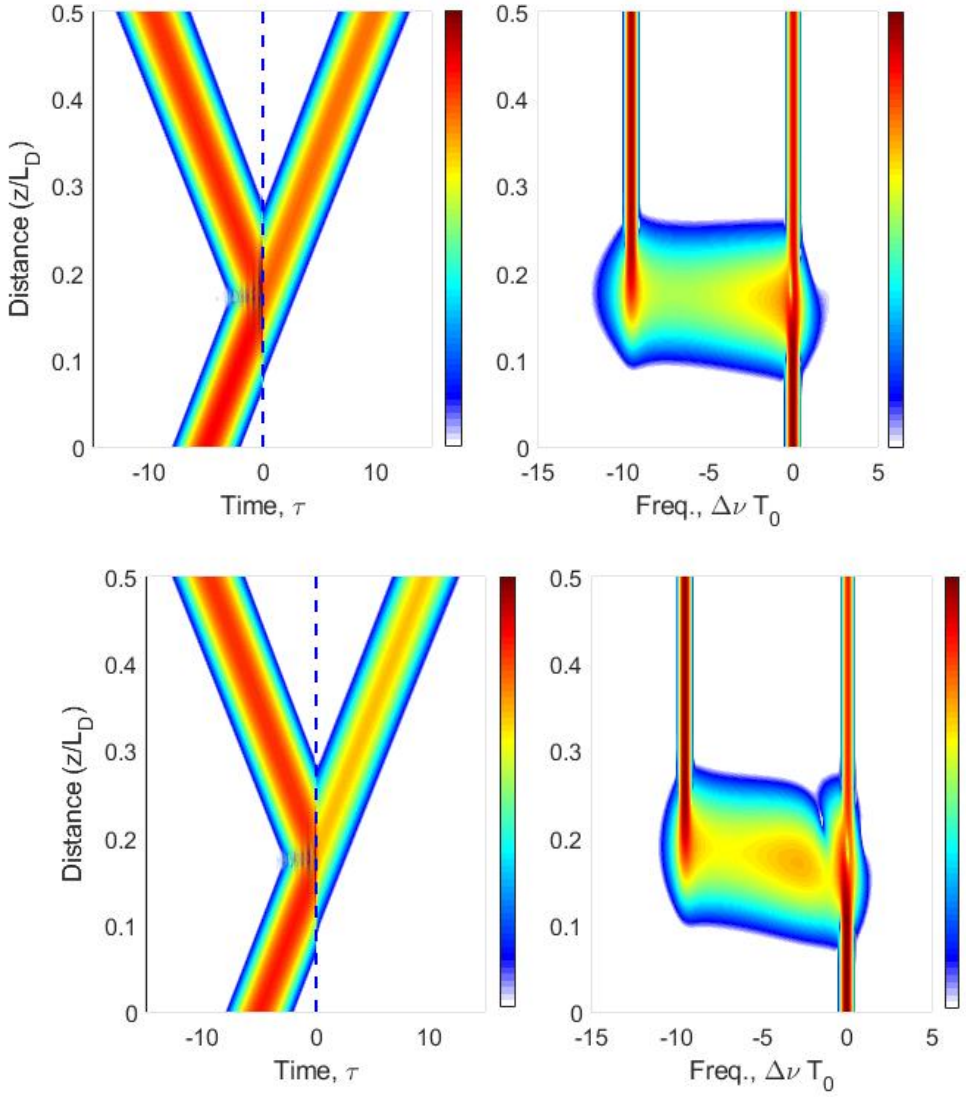

Figure 2. The reflection and refraction of a Gaussian pulse by a soliton that is 10 times (**top**) or 5 times (**bottom**) shorter than the pulse. The temporal (**left**) and spectral (**right**) intensities are shown along the fiber's length in both cases on a 40 dB colormap. A dashed vertical line marks the location of the soliton's peak in the moving frame.

2.2. Reflectivity of a Soliton

It turns out that the reflectivity of a soliton can be found in an analytic form with a simple trick. We can remove the second term in Equation (3) by shifting ω_0 from the probe's central frequency to the one for which $d = 0$. With this shift in the reference frequency ω_0, Equation (3) takes the form of a standard Schrödinger equation:

$$-i\frac{\partial A}{\partial \xi} = -\frac{1}{2}\frac{\partial^2 A}{\partial \tau^2} + V(\tau)A. \tag{4}$$

where $A(\xi, \tau)$ is the wave function and $V(\tau) = C_x \text{sech}^2(\tau/\tau_s)$ plays the role of a potential barrier.

Although Equation (4) resembles the Schrödinger equation of quantum mechanics (ξ plays the role of time), it does not contain $\hbar$ as expected for a classical problem. Nevertheless, it is useful because one can use relevant quantum results with only minor changes. Specifically, Equation (4) shows that the time-reflection problem is analogous to the scattering of a quantum particle from a potential barrier. As the potential V does not depend on ξ

in Equation (4), known solutions of the reflection and transmissions coefficients for specific barrier shapes can be directly applied to this classical problem.

For the "sech-shape" potential, the reflectivity of a plane wave, with the frequency shift δ_i from the reference frequency, can be written as [25]:

$$R(\delta_i) = \left[1 + \frac{\sinh^2(D)}{\cosh^2(\pi\sqrt{B-1}/2)}\right]^{-1}, \tag{5}$$

where $B = 8C_x\tau_s^2$ and $D = \pi\delta_i\tau_s$. Besides δ_i, R depends on the soliton's width, which sets the width of the potential barrier. The dependence of R on the frequency shift is shown in Figure 3 for three values of B. For all reasonable values of B, reflectivity is nearly 100% in the range $-4 < D < 4$, or for frequency shifts such that $|\delta_i| < 1/\tau_s$. This feature suggests that the use of narrower solitons would enhance the reflectivity over a wider frequency range. However, as we shall see later, Raman scattering becomes important for short pump pulses and needs to be taken into account.

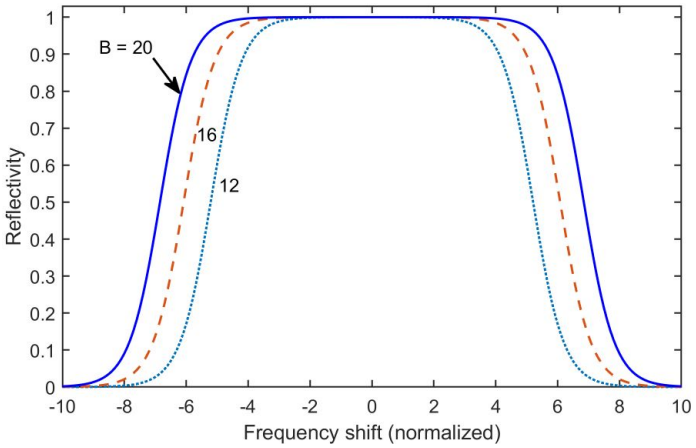

Figure 3. The frequency dependence of the reflectivity of a soliton for three values of the parameter B.

The reflectivity of a probe pulse can be found by considering each of its spectral components separately and integrating over all frequencies. For example, the amplitude of the reflected pulse after its generation can be calculated using

$$A_r(\tau) = \frac{1}{2\pi}\int_{-\infty}^{\infty}\sqrt{R(\delta_i)}e^{i\phi_r}\tilde{A}(\delta_i)e^{i\delta_i\tau}d\delta_i, \tag{6}$$

where $\tilde{A}(\delta_i)$ is the Fourier transform of the probe pulse and ϕ_r is the phase of the reflection coefficient.

2.3. Soliton-Based Waveguides

Similarly to the spatial case, time-domain TIR can be used to provide the temporal analog of optical waveguides, which confine beams spatially to a high-index core, sandwiched between two cladding layers. In the temporal case, a pulse would be confined within a moving time window, where the refractive index differs from the regions outside of that window [16]. When a probe pulse is located in the middle of two fundamental solitons acting as mirrors, it travels first toward one of these solitons and is totally reflected from it. The spectrum of the reflected pulse is shifted such that it slows down and moves away from this soliton. When the pulse arrives at the second soliton, it is reflected again through TIR, and its center frequency shifts back to the original value. This process repeats itself, trapping the pulse between the two solitons.

Figure 4 shows how such a waveguide functions by solving the NLS Equation (3) numerically, after it was modified to include the impact of both solitons:

$$\frac{\partial A}{\partial \xi} + d\frac{\partial A}{\partial \tau} + \frac{i}{2}\frac{\partial^2 A}{\partial \tau^2} = iC_x\left[\text{sech}^2\left(\frac{\tau - q}{\tau_s}\right) + \text{sech}^2\left(\frac{\tau + q}{\tau_s}\right)\right]. \quad (7)$$

It depicts the temporal (left) and spectral (right) evolution along the fiber's length when a Gaussian-shape probe pulse of width T_0 is located initially in the middle of two solitons, separated by 10 T_0. In normalized units, Equation (7) was solved with the initial amplitude $A(0,\tau) = \exp(-\tau^2/2)$ using the parameter values $d = 40$, $\tau_s = 0.1$ and $C_x = 1000$. Two solitons, located at $q = \pm 5$, were 10 times shorter than T_0. The probe's width is not limited to any specific value. As an example, when $T_0 = 1$ ps for probe pulses at a wavelengths near 1.1 μm, the required fiber's length is under 100 m. The wavelength of 100 fs pump pulses should be near 1.5 μm to ensure the anomalous GVD needed for the two solitons.

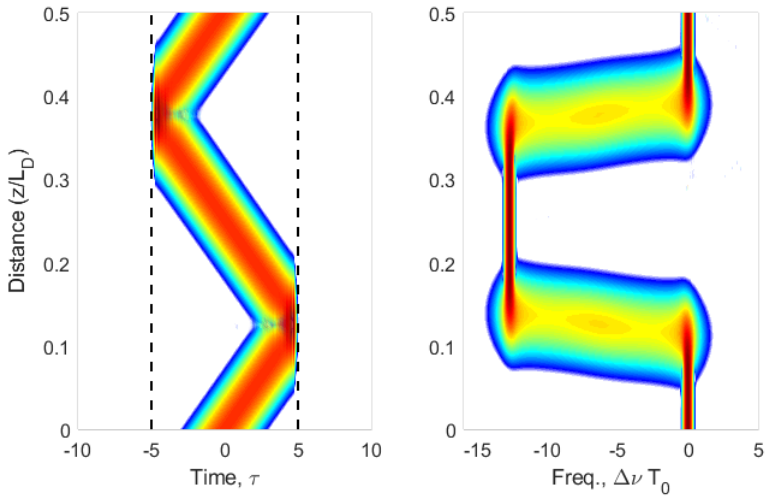

Figure 4. Evolution of the shape (**left** part) and spectrum (**right** part) of a Gaussian pulse inside a temporal waveguide formed by two solitons that act as 100% reflecting mirrors. Dashed vertical lines mark the core region of this waveguide.

3. Impact of Raman Scattering

So far, pump pulses have been assumed to form ideal solitons whose shape, width, and spectrum do not change with propagation inside an optical fiber. This is the case when pump pulses are not too short and their width exceeds a few picoseconds. However, shorter pump pulses (width 100 fs or less) are often employed in practice because their use reduces the length of fiber needed for experiments.

When an ultrashort pump pulse is used to create a moving index boundary, higher-order dispersive and nonlinear effects begin to affect the shape and spectrum of the soliton used to form this boundary. The most relevant higher-order nonlinear effect turns out to be a phenomenon known as intrapulse Raman scattering [20]. The spectrum of a femtosecond pump pulse is wide enough that its high-frequency components can transfer energy to the low-frequency components of the same pulse through Raman amplification. This process causes the soliton's spectrum to shift toward longer and longer wavelengths as it propagates along the fiber. In the presence of anomalous GVD, a red-shift in the soliton causes it to slow down (decelerate) along the fiber's length. The net effect is that the spatiotemporal boundary formed by the soliton does not remain stationary in any inertial frame moving with a constant speed. This section focuses on the impact of such a boundary on temporal reflection and waveguiding.

3.1. Evolution of Short Pump Pulses

The NLS Equation (1), governing the evolution of picosecond pump pulses inside an optical fiber, needs to be modified to include the effects of intrapulse Raman scattering. This is accomplished by changing the dispersive and nonlinear terms in this equation as follows [20]:

$$\frac{\partial A_p}{\partial z} + \sum_{m\geq 2} i^{m-1}\frac{\beta_{mp}}{2}\frac{\partial^m A_p}{\partial T^m} = i\gamma_p A_p \int_{-\infty}^{\infty} R(t')|A_p(z, T-t')|^2 dt', \tag{8}$$

where the sum includes multiple dispersion term,s and the nonlinear response function $R(t)$ has the form

$$R(t) = (1-f_R)\delta(t) + f_R h_R(t). \tag{9}$$

The first term in this equation corresponds to the Kerr effect. The second term accounts for the Raman effect through its fractional contribution f_R (about 18% for silica fibers); consult Ref. [20] for a functional form of the Raman response function $h_R(t)$.

Equation (8) can be solved numerically to reveal how intrapulse Raman scattering affects a soliton. An example is shown in Figure 5, where the evolution of the shape and spectrum of a 100 fs pump pulse is shown over the 60 m length of a silica fiber using $\beta_{2p} = -16$ ps^2/km, $\beta_{3p} = 0.1$ ps^2/km, and $\gamma_p = 1.3$ W^{-1}/km, values appropriate at a wavelength near 1.5-μm (terms with $m > 3$ were ignored). The initial amplitude was $A_p(0, T) = \sqrt{P_s}\,\mathrm{sech}(T/T_s)$, and the peak power P_s was chosen to ensure the formation of a fundamental soliton. As expected, the soliton's spectrum in part (b) shifts continuously toward the red side because of intrapulse Raman scattering. As a result of this shift, the soliton slows down, resulting in a bent trajectory, seen in part (a) of Figure 5. We refer to such a speed-changing soliton as the Raman soliton. If intrapulse Raman scattering is ignored by setting $f_R = 0$ in Equation (9), the soliton's trajectory would be vertical, indicating a constant speed of the soliton in the moving frame used here.

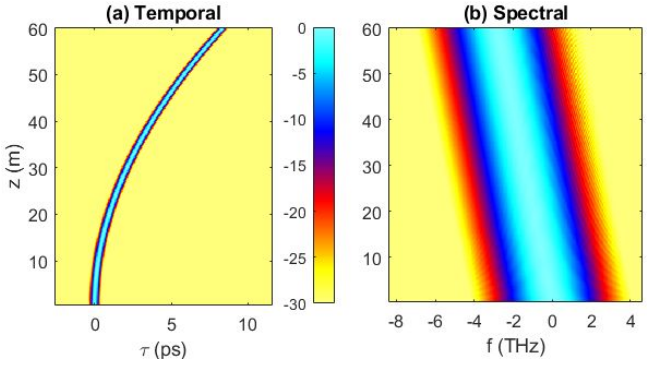

Figure 5. (**a**) The temporal and (**b**) spectral evolution of a 100 fs wide pump pulse inside a 60 m long silica fiber in the presence of intrapulse Raman scattering.

One can also solve Equation (8) with the variational method to obtain approximate analytic expressions for the spectral and temporal shifts of a Raman soliton. The solution has the form [20]

$$A_p(z, T) = \sqrt{P_s}\,\mathrm{sech}\left(\frac{T-q_s}{T_s}\right)e^{-i\Omega_s T + i\phi_s}. \tag{10}$$

This shows that the Raman soliton's shape and width, governed by $|A_p(z, T)|^2$, do not change, even though its peak shifts because of speed changes and its spectrum shifts toward the red side. Moreover, the Raman-induced frequency and temporal shifts vary with distance z and are given by

$$\Omega_s = -\frac{8T_R|\beta_{2p}|z}{15T_s^4}, \qquad q_s = \frac{4T_R\beta_{2p}^2 z^2}{15T_s^4}, \tag{11}$$

where T_R is a constant whose value (about 3 fs) depends on the Raman response function as $T_R = \int_0^\infty t\, h_R(t)\, dt$. The frequency shift varies linearly with z, but the temporal shift varies as z^2. This is indeed what is observed in Figure 5. Notice also that both shifts depend on the soliton's width as $1/T_s^4$, indicating that they increase rapidly as solitons become shorter.

3.2. Temporal Reflection and Focusing

To achieve temporal reflection, the speed difference between the pump and probe pulses should be relatively small [14]. One way to achieve this is to notice that a single-mode silica fiber has its zero-dispersion wavelength around 1310 nm, where β_2 vanishes. As β_2 has different signs on the opposite sides of this wavelength, for any wavelength of the pump, a wavelength exists on the opposite side that has the same group velocity. For example, if we choose the pump's wavelength at 1500 nm, the group velocity at 1145 nm matches that of the pump pulse. In practice, the wavelength of probe pulses should be in the range of 1145 ± 20 nm to ensure relatively high reflectivity.

One way to model the probe's evolution is to solve Equation (8) with the initial condition

$$A_p(0,t) = A_s(0,t) + A(0,t)\exp(-i\Delta\omega t), \tag{12}$$

where A_s and A are the envelope of the pump and probe pulses at $z = 0$, and $\Delta\omega$ is the frequency shift between the two pulses. This solution provides $A_p(z,t)$ at various distances inside the fiber. The pump and probe pulses can be separated by using a bandpass filter in the spectral domain. This approach requires long computing times because its temporal resolution scales inversely with $\Delta\omega$ and should be < 1 fs in practice.

When the spectra of pump and probe pulses are widely separated, one can employ Equation (8) to obtain two coupled NLS equations for the pump and probe pulses by using

$$A_p(z,t) = A_s(z,t) + A(z,t)\exp[i(\Delta\beta z - \Delta\omega t)], \tag{13}$$

where $\Delta\omega = \omega_0 - \omega_p$ is the frequency shift in the probe from the pump and $\Delta\beta$ is the corresponding change in its propagation constant. Substituting Equation (13) into Equation (8) and separating the terms in the two spectral regions, we obtain the following two equations:

$$\begin{aligned}\frac{\partial A_s}{\partial z} + \sum_{m\geq 2} i^{m-1}\frac{\beta_{mp}}{2}\frac{\partial^m A_s}{\partial T^m} &= i\gamma(1-f_R)(|A_s|^2 + 2|A|^2)A_s \\ &+ i\gamma f_R\int_{-\infty}^{\infty} h_R(t')(|A_s|^2 + |A|^2)A_s(t-t')dt',\end{aligned} \tag{14}$$

$$\begin{aligned}\frac{\partial A}{\partial z} + \sum_{m\geq 1} i^{m-1}\frac{\beta_m}{2}\frac{\partial^m A}{\partial T^m} &= i\gamma(1-f_R)(|A|^2 + 2|A_s|^2)A_s \\ &+ i\gamma f_R\int_{-\infty}^{\infty} h_R(t')(|A_s|^2 + |A|^2)A(t-t')dt'.\end{aligned} \tag{15}$$

The preceding equations can be simplified when probe pulses are much less intense than pump pulses (often the case in practice). In this situation, we retain the XPM term in Equation (15) but neglect the self-phase modulation term. As probe pulses are often wider than pump pulses, we can neglect higher-order dispersive effects for them. For the same reason, $h_R(t')$ in Equation (15) can be replaced with a delta function and the integral evaluated analytically. The probe's equation then takes the following simpler form [26]:

$$\frac{\partial A}{\partial z} + \Delta\beta_1\frac{\partial A}{\partial T} + \frac{i\beta_2}{2}\frac{\partial^2 A}{\partial T^2} = i(2-f_R)\gamma|A_s(z,T)|^2 A. \tag{16}$$

For the pump pulse, we can use Equation (8) when it is not affected by the probe pulse in a significant fashion.

To study the temporal reflection of a probe pulse from a Raman soliton, Equations (8) and (16) were solved numerically in a 2022 study [26] with the same parameter values used for Figure 5. The shape of the probe pulse at the input end of the fiber was Gaussian:

$$A(0,T) = \exp\left[-(T-T_d)^2/2T_0^2\right], \tag{17}$$

with $T_0 = 1$ ps and $T_d = 2.5$ ps. The parameter $\Delta\beta_1$ accounted for the probe's wavelength being longer by 10 nm from the speed-matching wavelength at 1145 nm of the silica fiber for 1500 nm pump pulses.

Figure 6 shows the evolution of a probe pulse and its temporal reflection from the Raman soliton, whose trajectory follows the dashed line. The probe pulse, delayed initially by 2.5 ps, travels faster than the soliton and catches up with it at a distance of about 10 m. After that distance, most of its energy is reflected; only a small fraction (<10%) is transmitted and appears on the other side of the pump pulse. The spectrum of the reflected pulse seen in part (b) is not only shifted by about 6 THz; it is also considerably wider than that of the probe pulse. Such spectral broadening does not occur for picosecond pump pulses, for which intrapulse Raman scattering plays a minor role. Notice also what happens in the time domain. The reflected pulse is narrower than the incident probe pulse and narrows further with propagation, exhibiting a kind of temporal focusing.

The behavior seen in Figure 6a can be understood as the temporal analog of a beam's focusing from a curved mirror and is another example of the concept of space–time duality. Since the soliton's trajectory is curved in a parabolic fashion, the probe pulse is "focused in time" as it is reflected by a parabolic mirror. More precisely, when the probe pulse interacts with the soliton through XPM, it becomes chirped and its spectrum broadens. With further propagation, this chirped pulse is compressed by the GVD of the fiber, resulting in temporal focusing. Compression by a factor of 10 was observed numerically [26] for wider probe pulses ($T_0 = 2.5$ ps).

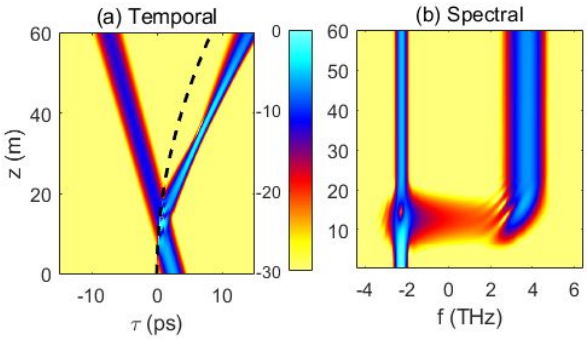

Figure 6. (**a**) The temporal and (**b**) spectral evolution of a 1 ps wide probe pulse reflecting from a 0.1 ps wide soliton. The dashed line shows the trajectory of the soliton. Adapted from Ref. [26].

3.3. Time-Domain Waveguiding

One should ask how intrapulse Raman scattering affects the formation of temporal waveguides, discussed in Section 2.2. As noted in Section 2.2, when two solitons moving with a constant speed travel inside an optical fiber, a probe pulse can be trapped between them by the TIR occurring at each soliton. However, if the speed of both solitons changes with distance because of Raman-induced spectral shifts, it is not evident that a waveguide can still form.

This issue was addressed in a 2023 study [27] by solving Equation (8) with an input in the form

$$A_p(0,T) = \sqrt{P_s}\left(\mathrm{sech}[(T-\tfrac{1}{2}T_g)/T_s] + e^{i\pi/2}\mathrm{sech}[(T+\tfrac{1}{2}T_g)/T_s]\right), \tag{18}$$

where T_g is the initial spacing (gap) between the two pump pulses of width T_s, whose peak powers were chosen such that they formed two fundamental solitons. The time gap T_g was much larger than the width T_s of the two solitons to prevent any nonlinear interaction between them [20]. The 90° phase shift between the two solitons was introduced to reduce their interaction further. The probe was still a Gaussian pulse with the initial amplitude given in Equation (17), but it was located in the middle of the two solitons ($T_d = 0$).

As a specific example, the pump–probe equations were solved numerically using $T_s = 0.2$ ps, $T_0 = 1$ ps, $T_g = 5$ ps, $\beta_2 = -\beta_{2p} = 14$ ps^2/km, and $\gamma = 2$ W^{-1}/km. Figure 7 shows the evolution of the pump (top) and probe (bottom) pulses over a 1 km long fiber, both in the time and frequency domains. As expected, the spectrum of pump pulses (part b) red-shifts because of intrapulse Raman scattering (spectral fringes result from interference). In the time domain (part a), the trajectories of both solitons are bent in a parabolic fashion because of deceleration caused by spectral red-shifts.

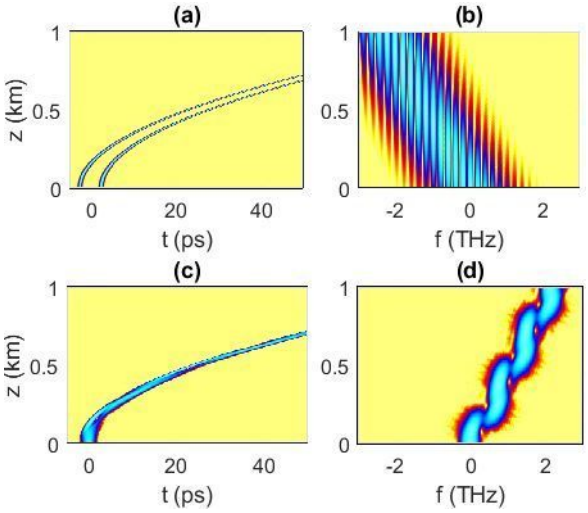

Figure 7. Temporal and spectral evolutions of the pump (**a,b**) and probe (**c,d**) pulses over a 1 km long fiber. The probe pulse is trapped within the temporal waveguide formed by two Raman solitons. Adapted from Ref. [27].

The evolution of the probe pulse in part (c) shows clearly that the probe is trapped within the temporal waveguide formed by two Raman solitons. In the absence of pump pulses, the probe's trajectory would be vertical, its spectrum would remain unchanged, and its width would increase because of dispersion. As the two solitons form a waveguide, the probe pulse is trapped between them and is forced to decelerate with them. In the spectral domain (part d), the probe's spectrum shifts toward higher frequencies (a blue-shift), and this shift is required for its speed to decrease. An interesting feature is that, although the pump's spectrum red-shifts linearly with distance, the probe's spectrum does not do so and exhibits a zigzag pattern toward the blue side. It turns out that the waveguide formed by the two Raman solitons is the temporal analog of a spatial waveguide with a curved core.

An approximate analytic treatment of such temporal waveguides has been carried out by working in a non-inertial frame in which both Raman solitons appear stationary [27]. Noticing that the Raman-induced time delay of the soliton in Equation (11) varies quadratically with distance, one can introduce a new time variable:

$$\tau' = \tau - a\xi^2, \quad a = 4T_R(\beta_{2p}L_D)^2/(15T_0T_s^4). \tag{19}$$

In this frame, the Raman solitons are stationary but Equation (4) is transformed into

$$-i\frac{\partial A}{\partial \xi} = -\frac{1}{2}\frac{\partial^2 A}{\partial \tau'^2} - 2ia\xi\frac{\partial A}{\partial \tau'} + V(\xi,\tau')A. \tag{20}$$

One can find temporal modes of this eigenvalue equation in the adiabatic approximation [27]. The term containing a leads to coupling among various waveguide modes, similar to the coupling introduced by the bending of a curved spatial waveguide. The resulting coupled-mode equations are useful for gaining physical insight into the numerical results shown in Figure 7.

3.4. Experimental Status

In general, the observation of temporal reflection from a soliton requires a short pump pulse and a probe pulse traveling at nearly the same speed at a different wavelength. However, even before this process was identified, it had occurred in many experiments on supercontinuum generation [28], where a higher-order soliton breaks into many fundamental solitons, which generate dispersive waves that can play the role of a low-energy probe pulses [20]. More direct evidence of temporal reflection has been seen in experiments that interpret it as reflection from an optical analog of the "event horizon" created by a soliton [21–24]. In these experiments, a high-index region, created inside an optical fiber by a soliton, reflects the probe with substantial frequency shifts.

As an example, one may cite the 2012 experiment [23], performed using a short microstructured fiber (only 1.1 m long), whose zero-dispersion wavelength was in the visible region near 710 nm. This feature allowed the use of 105 fs pulses at 810 nm for forming the Raman solitons in the anomalous-GVD region of the fiber. Probe pulses were launched in the normal-GVD region of the fiber at wavelengths near 620 nm so that they traveled at nearly the speed of pump pulses. When the wavelength of probe pulses was varied from 595 to 645 nm, either a blue-shift or a red-shift was observed for the reflected pulse, depending on whether the probe was traveling slower or faster than the soliton. These features agree with the discussion in Sections 2.2 and 3.2.

Clear evidence of the formation of a temporal waveguide by two Raman solitons was seen in a 2015 experiment through a pump–probe-type experiment [29]. A 29 m long photonic crystal fiber was employed with its zero-dispersion wavelength near 980 nm. The pump pulses were 250 fs wide, and their wavelength was tunable from 1000 to 1500 nm. The probe pulses were considerably wider, and their 802 nm wavelength was in the normal-GVD region of the fiber. Each pump pulse was split into two pulses, separated by 3.6 ps, using a setup similar to a Michelson interferometer. The probe pulses were synchronized such that each was located in the center of a pair of pump pulses at the input end of the fiber.

The peak power of the pump pulses was adjusted in the experiment to ensure that they propagated through the fiber as Raman solitons. Each probe pulse was found to be trapped within the so-called "solitonic cage", formed by the two Raman solitons that surrounded it. Even though the trapping was not interpreted as a temporal waveguide, spectral measurements showed clearly how the wavelength of the probe pulses shifted back and forth, in a fashion similar to that seen in Figure 4. Both the numerical and experimental results reported in Ref. [29] agree with the discussion of temporal waveguides in Sections 2.3 and 3.3. Such a waveguide is formed because of periodic TIR of the probe from the two solitons that surround it.

In a more recent experiment [30], temporal refraction of a probe soliton by a nonuniform train of solitons (called the soliton gas) was observed. When the probe passed through such a train of solitons, its frequency shifted owing to its refraction by the soliton train. The disordered nature of a soliton train can also lead to the temporal analog of Anderson localization under suitable conditions [31,32].

4. Waveguiding with a Single Soliton

As we saw in Section 2.3, a temporal waveguide generally requires two solitons, separated in time by a fixed interval, so that a probe pulse can remain confined between the two solitons. The discussion in Section 3.3 revealed how two Raman solitons, whose speed does not remain constant because of intrapulse Raman scattering, can still confine a probe

pulse between them through multiple reflections. However, a new kind of waveguiding has been discovered in the case of Raman solitons. It was found that a single Raman soliton can also guide a probe pulse along its trajectory through multiple reflections, and recent experiments have confirmed such predictions [33].

In the experiments, a short photonic crystal fiber (PCF) was used as a nonlinear dispersive medium for forming the temporal waveguide with a single Raman soliton. As the zero-dispersion wavelength of this PCF was 738 nm, short pump pulses were obtained from a mode-locked laser operating at 800 nm. Probe pulses were launched at a wavelength on the opposite side of the PCF's zero-dispersion wavelength such that their speed nearly matched the speed of the pump pulses.

4.1. Numerical Simulations

Figure 8 shows the results obtained numerically by solving the pump–probe equations, given in Equations (14) and (15), with the parameter values appropriate for the PCF used in the experiments. The 800 nm pump pulse was 110 fs wide and was launched with a 137 fs probe pulse at 683 nm. Both pulses had nearly the same speed at the input end of the fiber. The energy of the pump pulse was high enough to form a fourth-order soliton. The energy of probe pulses was a small fraction of this energy.

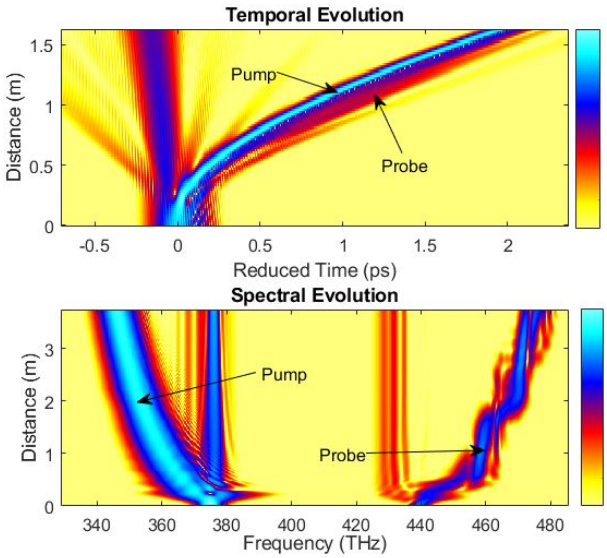

Figure 8. Numerical simulations (**top**) showing the Raman-induced guiding of a probe pulse by a single Raman soliton along its trajectory. The spectral evolution (**bottom**) shows the red and blue-shifts of the pump and probe pulses along the fiber's length. Adapted from Ref. [33].

Several things are noteworthy in Figure 8. First, the higher-order soliton undergoes fission within the first 20 cm of the fiber (top panel) such that an ultrashort fundamental soliton is formed [20]. This soliton undergoes a large spectral redshift (>40 THz, see bottom panel) through intrapulse Raman scattering. The speed of the Raman soliton keeps decreasing because of its deceleration, resulting in a bent trajectory in the time domain. The probe pulse follows this trajectory through multiple temporal reflections while changing its frequency in a zigzag fashion toward the blue side (see bottom panel). At the end of the fiber, the spectra of both pulses have shifted by about 40 THz. In the time domain, the probe pulse remains close to the Raman soliton but does not overlap with it.

One can view the Raman-induced waveguiding process as a cascade of temporal reflections along the fiber's length. As the pump pulse slows down near the front end of the fiber, the probe reflects from it for the first time, and its spectrum blue-shifts to match the speed of pump pulse at that time. As the pump pulse keeps slowing down, a second reflection occurs that shifts the probe's frequency further to the blue side. This process keeps repeating along the fiber's length. Such a cascade of temporal reflections ensures

that the pump and probe pulses move together along the entire length of the fiber. This interpretation is justified by the zigzag pattern of the probe's blue-shifts seen in Figure 8.

4.2. Experimental Results

Figure 9 shows the experimental setup used in Ref. [33] to observe the waveguiding of probe pulses by a single Raman soliton. An optical parametric amplifier (OPA) provided 683 nm probe pulses that were combined with 800 nm pump pulses, delayed suitably using a translation stage. The resulting beam was focused onto a 3.75 m long PCF, and its output was characterized with a spectrometer. A linear polarizer before the PCF ensured that the two pulses had the same polarization direction, which was aligned with a principal axis of the PCF. A half-wave plate was used in the pump's path to change the peak power of the pump pulses.

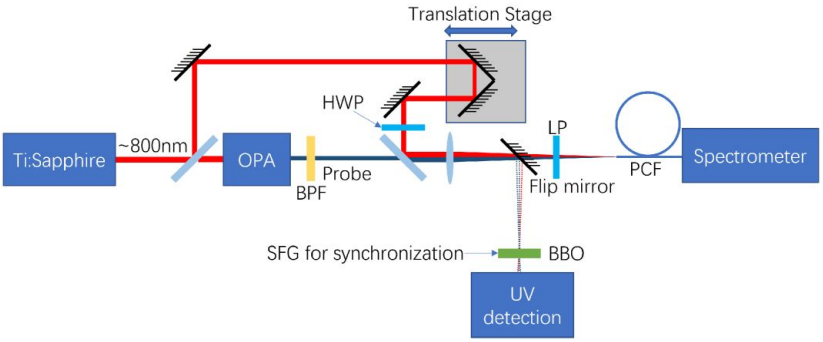

Figure 9. Schematic of experimental setup. BPF: bandpass filter; HWP: half-wave plate; LP: linear polarizer.

Figure 10 shows the spectra measured at the PCF's output in three different situations. When only pump pulses were launched, the spectrum [blue trace in part (a)] contained two dominant peaks, one centered at the input wavelength of 800 nm and the other at 866 nm. The 866 nm peak corresponds to the Raman soliton, formed after a short distance into the PCF. Intrapulse Raman scattering had the greatest impact on this soliton, and its spectrum was red-shifted by 66 nm at the PCF's output end. When only probe pulses were launched at 683 nm, a single peak at this wavelength was observed [red trace in part (a)], as expected for such low-energy pulses.

When both the pump and probe pulses were launched together into the PCF, the output spectrum, shown in part (b) of Figure 10, had a new blue-shifted peak at 631 nm that contained a large fraction of the probe's energy. The 52 nm blue-shift in the probe was induced by the Raman soliton, which guided the probe pulse along its own trajectory, as seen in Figure 8. According to numerical simulations, the probe's blue-shift increased in a discrete step-like fashion inside the PCF. This feature can be understood by recalling that the probe pulse reflects from the Raman soliton several times in a cascaded fashion (see Figure 8). The spectral shift is different each time because it depends on the speed of the Raman soliton at the location where the collision of the probe with the Raman soliton occurs inside the fiber.

The trapping of weak pulses (dispersive waves) by optical solitons has been noted in several different contexts, including supercontinuum generation [34–39]. The blue-shift in a probe pulse, trapped by a Raman soliton, was observed as early as 2002, using a relatively long dispersion-shifted fiber [34]. However, it was not realized that this trapping was due to multiple reflections of the probe pulse from a decelerating Raman soliton with a curved trajectory. As seen in Figure 8, Trapping of weak pulses (dispersive waves) the probe pulse follows the trajectory taken by the Raman soliton by shifting its frequency to the blue side through multiple reflections such that the two pulses move at nearly the same speed and thus appear trapped.

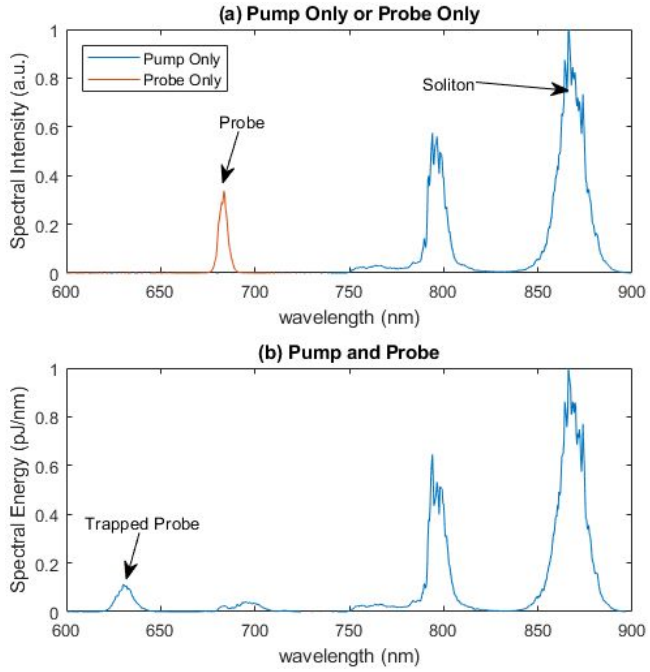

Figure 10. The measured spectra when (**a**) only the pump or probe pulse and (**b**) both the pump and probe pulses were sent through the PCF. Adapted from Ref. [33].

4.3. Probing of Soliton's Trajectory

As seen in Figure 5, the trajectory of a Raman soliton bends toward the right side because of its deceleration induced by a linearly increasing red-shift in the soliton's spectrum. Such temporal and spectral shifts in a Raman soliton, occurring inside any optical fiber, cannot be measured directly, unless one employs a cut-back method in which the fiber's length is reduced successively by cutting it. Such a technique is not only cumbersome but also destroys the fiber.

The experimental setup shown in Figure 9 can be used to deduce the temporal and spectral shifts in a Raman soliton at any distance within the fiber from the spectral measurements made only at the end of the fiber. Figure 11 shows the underlying idea schematically using three probe pulses with different initial delays. Even though only a single temporal reflection takes place, the resulting spectral shifts at the output of the fiber are different because these shifts depend on the speed of the Raman soliton at the precise location where probe pulse collides with the Raman soliton inside the fiber. The three probe pulses differ only in their relative delays from the pump pulse launched into the fiber. The wavelength of each reflected pulse at the fiber's output depends on the probe's initial relative delay at the input end. By varying this relative delay and measuring the reflected pulse's spectrum as a function of the delay, one can deduce how the frequency and speed of the Raman soliton evolve inside the fiber.

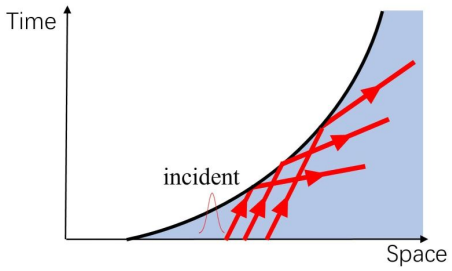

Figure 11. A schematic showing the temporal reflection of three probe pulses by a Raman soliton for different initial delays.

As an example, Figure 12 shows the numerically simulated output spectra of a 645 nm probe pulse for initial relative delays in the range of 0 to 2.5 ps. For small delays, temporal reflection leads to the blue-shifted peak seen on the left. As the delay becomes larger, the probe's blue-shift becomes smaller and eventually disappears. This behavior can be understood from Figure 11. As the delay increases, the collision between the probe and soliton occurs after a longer distance into the fiber. When the delay is large enough, the two never collide, and temporal reflection ceases to occur.

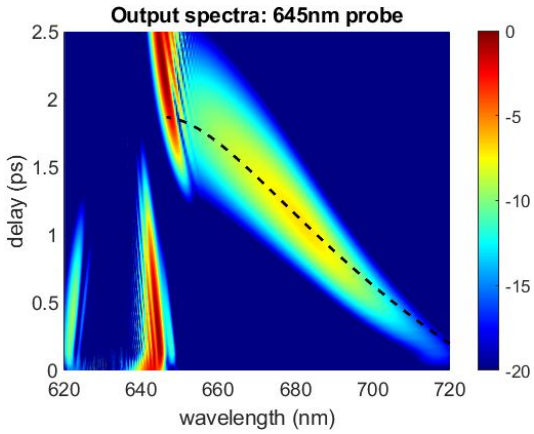

Figure 12. The output spectra of a 645 nm probe pulse for different initial pump–probe delays (probe pulses were delayed). The dashed line corresponds to the probe's peak. Adapted from Ref. [40].

In a 2023 experiment [40], the measured output spectra matched the pattern seen in Figure 12 reasonably well. However, probe pulses at three different probe wavelengths were needed to cover the entire trajectory of the Raman soliton. The delay dependence of the reflected pulse's wavelength at the PCF's output was used to deduce the speed of the Raman soliton at the location of its collision with the probe pulse, which, in turn, was used to calculate the soliton's red-shift at that location. The results agreed well with theoretical predictions based on Equation (11).

4.4. Impact of Soliton's Parameters

The results discussed so far in this section were obtained for pump pulses of a specific width, assuming that they were nearly chirp-free. Also, the probe pulses were delayed initially and were traveling faster than the pump pulses. One should ask what happens when input pump pulses are chirped and have a different width. One can also change the wavelength of a probe pulse such that they are launched ahead of the pump pulse and travel slower than pump pulses. This section focuses on a few specific situations to reveal novel effects that may occur.

As an example, Figure 13 shows the numerical results for 655 nm probe pulses (spectral width of 5 nm) launched with 800 nm pump pulses (width 30 fs) that were delayed initially by 0.33 ps into the same PCF used for the experiments in Section 4.2. Nothing happens to the probe pulse, until it collides with the Raman soliton at a distance of 0.25 m, resulting in temporal reflection. The reflected pulse travels faster than the probe pulse because its spectrum has been red-shifted by more than 20 THz from that of the probe. The wide spectral peak, appearing after 0.25 m and located near 435 THz in Figure 13, corresponds to this reflected pulse. In the time domain, this pulse spreads with further propagation because of a large normal GVD of the fiber at its wavelength.

The transmitted part of the probe pulse collides with the pump pulse a second time at a distance of about 2.5 m, producing a blue-shifted reflected pulse. The reason behind the blue-shift can be understood when we take into account the Raman-induced deceleration of the Raman soliton. During the first collision, this soliton is traveling faster than the probe. In contrast, it slows down so much at a distance of 2.5 m that its speed becomes smaller than that of the probe. The nature of frequency shift during temporal reflection depends

on the relative probe-soliton speed (sign of $\Delta\beta_1$); a blue-shift occurs when probe travels faster than the pump [14]. As we saw earlier, such multiple reflections lead to guiding of the probe pulse by the Raman soliton [33].

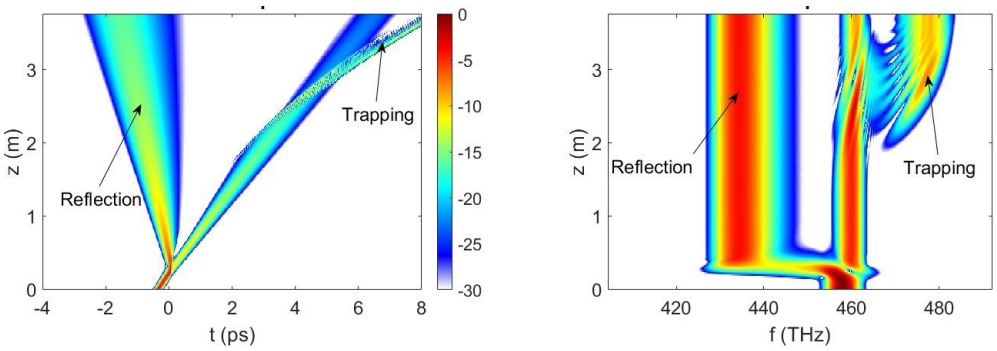

Figure 13. The temporal (**left**) and spectral (**right**) evolution of a probe pulse simulated numerically over the fiber's length. The pump pulse was delayed initially by 0.33 ps.

Recall that spectral shifts produced during temporal reflections depend on the location within the fiber where the pump and probe pulses collide. This location can be controlled by changing the initial relative delay between the two pulses. Figure 14 shows the probe's spectra obtained numerically for different pump–probe delays. Three main spectral bands can be seen in this figure. The central band, located near 650 nm, corresponds to the input probe pulse. The blue-shifted spectral band on the left results from trapping (or guiding) of the probe by the soliton through multiple reflections. The red-shifted spectral band on the right corresponds to the reflected pulse generated during the first collision of the probe. This red-shift becomes smaller for loner delays because the Raman soliton slows down as it propagates down the fiber. A larger initial delay forces the collision to occur at a longer distance, where the soliton's speed is closer to that of the probe, resulting in a smaller frequency shift. Experiments carried out with a PCF using the setup shown in Figure 9 confirm the behavior seen in Figure 14.

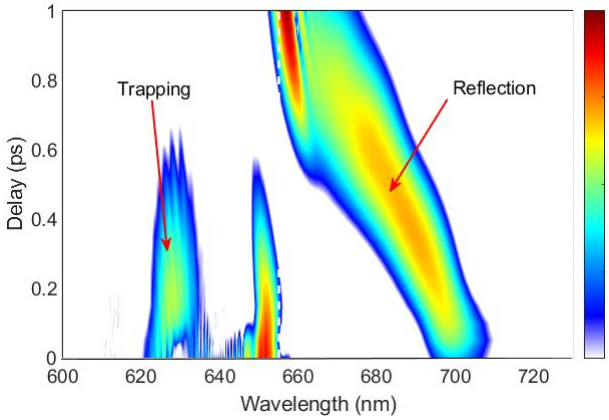

Figure 14. The simulated output spectra of a 645 nm probe pulse for different initial pump–probe delays. The pump pulses were delayed in this case. Adapted from Ref. [41].

The case of chirped pump pulses is also interesting. In a 2024 experiment [41], a pulse shaper based on two prisms and a mirror was used for this purpose. The measured width of chirped pump pulses (about 100 fs) corresponded to adding 1130 fs^2 of GVD to each 800 nm pump pulse. The experimental results for such chirped pump pulses are shown in Figure 15 using 655 nm probe pulses delayed suitably from pump pulses. Figure shows the probe's output spectra, measured by varying its initial delay from the pump in the 0 to 1 ps range, on a 20 dB intensity scale.

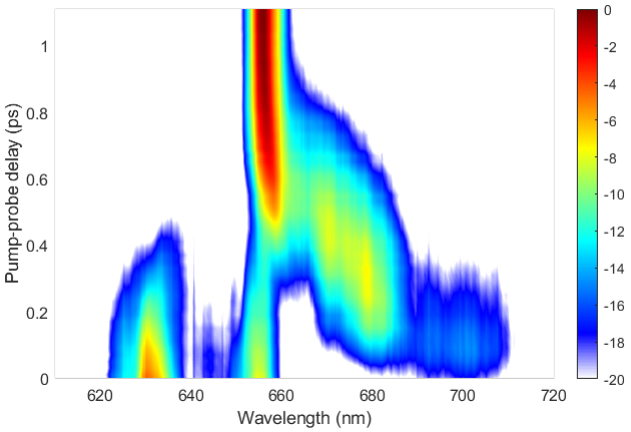

Figure 15. The measured probe spectra for chirped pump pulses as relative pump–probe delay is varied from 0 to 1 ps. Adapted from Ref. [41].

The experimental probe spectra in Figure 15 show features similar to those seen in Figure 14 for unchirped pump pulses, with some differences resulting from the chirping of pump pulses. Although three spectral bands are seen in both cases, a new spectral band appears near 700 nm in Figure 15 for small pump–probe delays. Clearly, a Raman soliton evolves differently because of an initial chirp imposed on the pump pulse. To confirm this, numerical simulations were performed using the measured shape and phase of input pump pulses, and the results are shown in Figure 16.

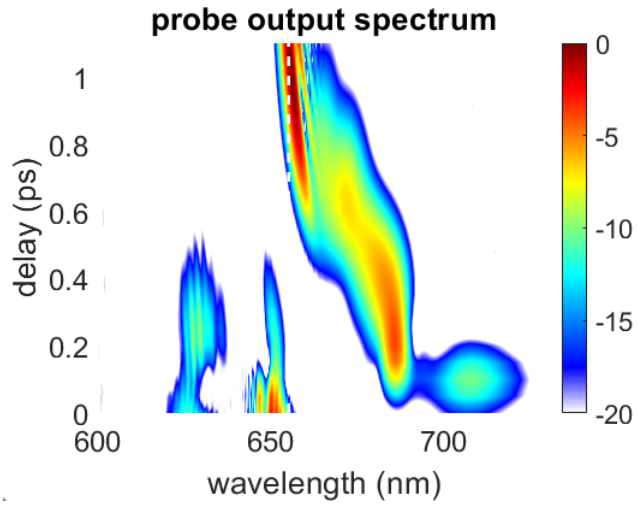

Figure 16. The simulated probe spectra in the experimental situation of Figure 15.

A comparison of the probe spectra in Figure 16 with the experimental results in Figure 15 shows relatively good agreement. In both cases, two reflected spectral bands are seen on the red side of the 655 nm probe band when the relative pump–probe delay is small. In both simulations and experiments, the red-shift in the main reflection peak decreases as the delay is increased, and this peak eventually merges with the spectrum of the incident probe pulse. The second reflection peak in Figure 16 at wavelengths near 700 nm is present for only small delays and disappears as the delay increases. This is also what was observed experimentally in Figure 15.

Numerical simulations were used to verify that double reflection indeed occurs for a pump–probe delay of $<$0.2 ps. The temporal and spectral evolution of the probe pulse is shown in Figure 17 over the first 1 m of the PCF for a pump–probe delay of 0.15 ps. As seen in this figure, the probe collides with the pump pulse within the first 10 cm of the PCF. At this point, the probe pulse splits into three parts. Only a small fraction of the probe's energy

is transmitted. Most of its energy appears in the form of two reflected pulses, whose spectra are red-shifted by different amounts (about 20 and 40 THz). As both pulses are traveling in the normal-GVD region of the fiber, their speeds increase by different amounts. The process of double reflection can be understood from Ref. [42], where it was found that an intense chirped pulse splits into two soliton-like pulses. Collision of the probe with these two closely spaced solitons is responsible for the two reflection pulses seen in Figure 17. The main conclusion is that temporal reflection is quite sensitive to parameters such as the width, chirp, and initial delay of pump pulses.

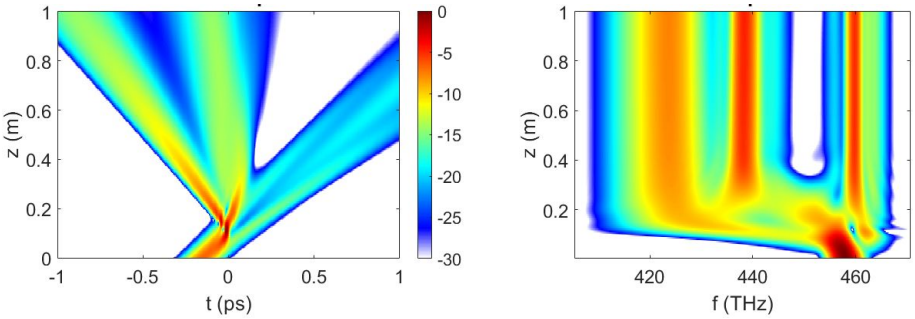

Figure 17. Temporal (**left**) and spectral (**right**) evolution of probe pulses showing double temporal reflection in the experimental situation of Figure 15.

5. Concluding Remarks

This review focused on novel phenomena that emerge when ultrashort optical pulses propagate through a nonlinear dispersive medium, such as an optical fiber. These phenomena occur when pump pulses propagate as optical solitons and modulate the fiber's refractive index through the optical Kerr effect, both in space and time, in a traveling-wave fashion. When the width of the pump pulses exceeds a few picoseconds, the shape, width, and spectrum of the solitons do not change with propagation along an optical fiber. This case was discussed first to introduce basic concepts such as the temporal reflection, total internal reflection, and time-domain waveguiding of probe pulses launched into the same fiber at a wavelength different from that of the pump.

Shorter pump pulses (width 100 fs or less) are often employed in practice because their use reduces the length of fiber needed for experiments. In this situation, higher-order effects begin to affect the shape and spectrum of each soliton. The most relevant higher-order nonlinear effect is the process of intrapulse Raman scattering. This process shifts the soliton's spectrum toward longer wavelengths in a continuous fashion, which, in turn, causes it to decelerate, as the soliton propagates down the fiber. Such a slowing down of the Raman soliton affects both the temporal reflection of probe pulses and their waveguiding when two closely spaced Raman solitons are used to confine them. At the same time, it can lead to novel effects such as temporal focusing of the reflected probe and waveguiding by a single variable-speed Raman soliton. Recent experimental results were also discussed in this context.

As a potential application of temporal refection and waveguiding, it was shown that temporal reflection can be used to deduce the spectral shifts in and speed changes of a Raman soliton, occurring all along an optical fiber, from the spectral measurements made only at the end of that fiber. Another application of temporal refection would be to shift the wavelength of low-energy pulses toward the blue side in a tunable fashion using intense pump pulses at a different wavelengths. Although four-wave mixing can also be used for this purpose, its use requires phase matching. Intrapulse Raman scattering does not require phase matching and shifts the wavelength of weak probe pulses toward the blue side by transferring the pump's red-shift to the probe as a blue-shift.

Funding: This research was funded in part by U.S. National Science Foundation grant number ECCS-1933328.

Informed Consent Statement: Not applicable.

Data Availability Statement: Data are contained within the article.

Acknowledgments: The author is thankful to his collaborators, William Donaldson, Brent Plansinis, and Junchi Zhang, for working with him on the topics covered in this review. He also thanks Guy Millot for his hospitality at the University of Burgundy, where this review was finalized.

Conflicts of Interest: The author declares no conflicts of Interest.

References

1. Gaafar, M.A.; Baba, T.; Eich, M.; Petrov, A.Y. Front-induced transitions. *Nat. Photonics* **2019**, *13*, 737–748. [CrossRef]
2. Caloz, C.; Deck-Léger, Z. Spacetime metamaterials—Part I: General concepts. *IEEE Trans. Antennas Propag.* **2019**, *68*, 1569–1582. [CrossRef]
3. Caloz, C.; Deck-Léger, Z. Spacetime metamaterials—Part II: Theory and applications. *IEEE Trans. Antennas Propag.* **2019**, *68*, 1583–1598. [CrossRef]
4. Li, H.; Alù, A. Temporal switching to extend the bandwidth of thin absorbers. *Optica* **2021**, *8*, 24–29. [CrossRef]
5. Galiffi, E.; Tirole, R.; Yin, S.; Li, H.; Vezzoli, S.; Huidobro, P.A.; Silveirinha, M.G.; Sapienza, R.; Alù, A.; Pendry, J.B. Photonics of time-varying media. *Adv. Photonics* **2022**, *4*, 014002. [CrossRef]
6. Boltasseva, A.; Shalaev, V.M.; Segev, M. Photonic time crystals: From fundamental insights to novel applications: Opinion. *Opt. Mater. Express* **2024**, *14*, 592–597. [CrossRef]
7. Morgenthaler, F.R. Velocity modulation of electromagnetic waves. *IRE Trans. Microw. Theory Tech.* **1958**, *6*, 167–172. [CrossRef]
8. Sharabi, Y.; Dikopoltsev, A.; Lustig, E.; Lumer, Y.; Segev, M. Spatiotemporal photonic crystals. *Optica* **2022**, *9*, 585–592. [CrossRef]
9. Wang, X.; Mirmoosa, M.S.; Asadchy, V.S.; Rockstuhl, C.; Fan, S.; Tretyakov, S.A. Metasurface-based realization of photonic time crystals. *Sci. Adv.* **2023**, *9*, eadg7541. [CrossRef]
10. Lustig, E.; Segal, O.; Saha, S.; Fruhling, C.; Shalaev, V.M.; Boltasseva, A.; Segev, M. Photonic time-crystals—Fundamental concepts. *Opt. Express* **2023**, *31*, 9165–9170. [CrossRef] [PubMed]
11. Bacot, V.; Labousse, M.; Eddi, A.; Fink, M.; Fort, E. Time reversal and holography with spacetime transformations. *Nat. Phys.* **2016**, *12*, 972–977. [CrossRef]
12. Moussa, H.; Xu, G.; Yin, S.; Galiffi, E.; Ra'di, Y.; Alù, A. Observation of temporal reflection and broadband frequency translation at photonic time interfaces. *Nat. Phys.* **2023**, *19*, 863–868. [CrossRef]
13. Dong, Z.; Li, H.; Wan, T.; Liang, Q.; Yang, Z.; Yan, B. Quantum time reflection and refraction of ultracold atoms. *Nat. Photonics* **2024**, *18*, 68–73. [CrossRef]
14. Plansinis, B.W.; Donaldson, W.R.; Agrawal, G.P. What is the temporal analog of reflection and refraction of optical beams? *Phys. Rev. Lett.* **2015**, *115*, 183901. [CrossRef]
15. Biancalana, F.; Amann, A.; Uskov, A.V.; O'Reilly, E.P. Dynamics of light propagation in spatiotemporal dielectric structures. *Phys. Rev. E* **2007**, *75*, 046607. [CrossRef] [PubMed]
16. Plansinis, B.W.; Donaldson, W.R.; Agrawal, G.P. Temporal waveguides for optical pulses. *J. Opt. Soc. Am. B* **2016**, *33*, 1112–1119. [CrossRef]
17. Plansinis, B.W.; Donaldson, W.R.; Agrawal, G.P. Cross-phase-modulation-induced temporal reflection and waveguiding of optical pulses. *J. Opt. Soc. Am. B* **2018**, *35*, 436–445. [CrossRef]
18. Zhang, J.; Donaldson, W.R.; Agrawal, G.P. Temporal reflection and refraction of optical pulses inside a dispersive medium: An analytic approach. *J. Opt. Soc. Am. B* **2021**, *38*, 997–1003. [CrossRef]
19. Zhang, J.; Donaldson, W.R.; Agrawal, G.P. Impact of the boundary's sharpness on temporal reflection in dispersive media. *Opt. Lett.* **2021**, *46*, 4053–4056. [CrossRef]
20. Agrawal, G.P. *Nonlinear Fiber Optics*, 6th ed.; Academic Press: Cambridge, MA, USA, 2019.
21. Philbin, T.G.; Kuklewicz, C.; Robertson, S.; Hill, S.; Konig, F.; Leonhardt, U. Fiber-optical analog of the event horizon. *Science* **2008**, *319*, 1367–1370. [CrossRef] [PubMed]
22. Demircan, A.; Amiranashvili, S.; Steinmeyer, G. Controlling light by light with an optical event horizon. *Phys. Rev. Lett.* **2011**, *106*, 163901. [CrossRef] [PubMed]
23. Tartara, L. Frequency shifting of femtosecond pulses by reflection at solitons. *IEEE J. Quantum Electron.* **2012**, *48*, 1439–1442. [CrossRef]
24. Webb, K.E.; Erkintalo, M.; Xu, Y.; Broderick, N.G.R.; Dudley, J.M.; Genty, G.; Murdoch, S.G. Nonlinear optics of fibre event horizons. *Nat. Commun.* **2014**, *5*, 4969. [CrossRef]
25. Landau, L.D.; Lifshitz, E.M. *Quantum Mechanics: Non-Relativistic Theory*; Elsevier: Amsterdam, The Netherlands, 2013; Volume 3, pp. 79–81.
26. Zhang, J.; Donaldson, W.R.; Agrawal, G.P. Temporal reflection of an optical pulse from a short soliton: Impact of Raman scattering. *J. Opt. Soc. Am. B* **2022**, *39*, 1950–1957. [CrossRef]
27. Zhang, J.; Donaldson, W.R.; Agrawal, G.P. Raman-induced mode coupling in temporal waveguides formed by short solitons. *Phys. Rev. A* **2023**, *107*, 033512. [CrossRef]

28. Dudley, J.M.; Genty, G.; Coen, S. Fibre supercontinuum generation overview. In *Supercontinuum Generation in Optical Fibers*; Dudley, J.M., Taylor, J.R., Eds.; Cambridge University Press: Cambridge, UK, 2010; pp. 52–61.
29. Wang, S.F.; Mussot, A.; Conforti, M.; Zeng, X.L.; Kudlinski, A. Bouncing of a dispersive wave in a solitonic cage. *Opt. Lett.* **2015**, *40*, 3320–3323. [CrossRef] [PubMed]
30. Suret, P.; Dufour, M.; Roberti, G.; El, G.; Copie, F.; Randoux, S. Soliton refraction by an optical soliton gas. *Phys. Rev. Res.* **2023**, *5*, L042002. [CrossRef]
31. Sharabi, Y.; Lustig, E.; Segev, M. Disordered photonic time crystals. *Phys. Rev. Lett.* **2021**, *126*, 163902. [CrossRef]
32. Eswaran, K.S.; Kopaei, A.E.; Sacha, K. Anderson localization in photonic time crystals. *arXiv* **2024**, arXiv:2410.23095.
33. Zhang, J.; Donaldson, W.R.; Agrawal, G.P. Experimental observation of a Raman-induced temporal waveguide. *Phys. Rev. A* **2023**, *107*, 063518. [CrossRef]
34. Nishizawa, N.; Goto, T. Pulse trapping by ultrashort soliton pulses in optical fibers across zero-dispersion wavelength. *Opt. Lett.* **2002**, *27*, 152–154. [CrossRef]
35. Austin, D.R.; de Sterke, C.M.; Eggleton, B.J.; Brown, T.G. Dispersive wave blue-shift in supercontinuum generation. *Opt. Express* **2006**, *14*, 11997–12007. [CrossRef] [PubMed]
36. Travers, J.C.; Taylor, J.R. Soliton trapping of dispersive waves in tapered optical fibers. *Opt. Lett.* **2009**, *34*, 115–117. [CrossRef] [PubMed]
37. Hill, S.; Kuklewicz, C.E.; Leonhardt, U.; König, F. Evolution of light trapped by a soliton in a microstructured fiber. *Opt. Express* **2009**, *17*, 13588–13601. [CrossRef] [PubMed]
38. Judge, A.C.; Bang, O.; de Sterke, C.M. Theory of dispersive wave frequency shift via trapping by a soliton in an axially nonuniform optical fiber. *J. Opt. Soc. Am. B* **2010**, *27*, 2195–2202. [CrossRef]
39. Robertson, S.; Leonhardt, U. Frequency shifting at fiber-optical event horizons: The effect of Raman deceleration. *Phys. Rev. A* **2010**, *81*, 063835. [CrossRef]
40. Zhang, J.; Donaldson, W.R.; Agrawal, G.P. Probing the decelerating trajectory of a Raman soliton using temporal reflection. *Opt. Express* **2023**, *31*, 27621–27632. [CrossRef]
41. Zhang, J.; Donaldson, W.R.; Agrawal, G.P. Temporal reflection from short pump pulses inside a dispersive nonlinear medium: The impact of pump parameters. *J. Opt. Soc. Am. B* **2024**, *41*, 1836–1846. [CrossRef]
42. Kaup, D.J.; El-Reedy, J.; Malomed, B.A. Effect of a chirp on soliton production. *Phys. Rev. E* **1994**, *50*, 1635–1637. [CrossRef] [PubMed]